The Astrophysical Journal Letters, 880:L23 (6pp), 2019 August 1 https://doi.org/10.3847/2041-8213/ab2fd4

GW170817 Afterglow Reveals that Short Gamma-Ray Bursts are Neutron Star Mergers

Yiyang Wu and Andrew MacFadyen
Center for Cosmology and Particle Physics, New York University, USA
Received 2019 May 7; revised 2019 June 30; accepted 2019 July 6; published 2019 July 30

Abstract

We systematically investigate the outflow structure of GW170817 in comparison with a sample of 27 cosmological short gamma-ray bursts (GRBs) by modeling their afterglow light curves. We find that cosmological short GRBs share the same outflow structures with GW170817, relativistic structured jets. The jet opening angle of GW170817 is $6.3^{+1.1}_{-0.6}{}^{\circ}$, which is consistent with that of cosmological short GRBs ($\theta_0 = 6.^{\circ}9 \pm 2.^{\circ}3$). Our analysis indicates that GW170817 is viewed off-axis ($\theta_{\rm obs} = 30^{+7}_{-4}{}^{\circ}$), while cosmological short GRBs are viewed on-axis ($\theta_{\rm obs} \lesssim \theta_0$). The exceptional properties of the GW170817 afterglow can be explained by the difference in observation angle alone. We demonstrate that the light curves of the GW170817 afterglow, if viewed on-axis, are consistent with those of cosmological short GRBs. Other properties of GW170817, such as Lorentz factor $\Gamma \approx 150$, spectral index $p \approx 2.15$, isotropic equivalent energy $E_{\rm iso} \approx 8 \times 10^{52}$ erg, and interstellar medium density $n_0 \approx 10^{-2}$ proton cm^{-3}, fit well within the ranges of those of cosmological short GRBs. The similarity between the GW170817 outflow structure and those of cosmological short GRBs indicates that cosmological short GRBs are likely neutron star mergers.

Key words: gamma-ray burst: general – gravitational waves – stars: neutron

1. Introduction

On 2017 August 17, LIGO/Virgo detected the first binary neutron star (BNS) merger event, known as GW170817 (Abbott et al. 2017). Approximately 1.7 s later, the *Fermi* space telescope detected a weak short-duration gamma-ray burst (GRB), GRB170817A, with an inferred sky location coinciding with that of GW170817 (Goldstein et al. 2017; Savchenko et al. 2017). After intensive multiband monitoring, a long-lived GRB afterglow was detected at radio, optical, and X-ray wavelengths (Alexander et al. 2017, 2018; Haggard et al. 2017; Hallinan et al. 2017; Kasliwal et al. 2017; Margutti et al. 2017, 2018; Troja et al. 2017; Dobie et al. 2018; Lyman et al. 2018; Mooley et al. 2018b, 2018c; Nynka et al. 2018; Piro et al. 2018; Resmi et al. 2018; Ruan et al. 2018; van Eerten et al. 2018; Lamb et al. 2019).

Compared to classical short GRBs, the γ-ray emission and the afterglow from GW170817 displayed exceptional properties. Located in NGC 4993, an elliptical galaxy at a distance of 39.5 Mpc ($z = 0.00973$), it is the closest burst among short GRBs with host galaxy identifications and has the lowest total gamma-ray energy $\sim 10^{46}$–10^{47} erg (Fong et al. 2017; Goldstein et al. 2017; Savchenko et al. 2017). For comparison, classical short GRBs are at cosmological distance and typically have γ-ray energies of $\sim 10^{50}$–10^{52} erg (Fong et al. 2015). The afterglow from GW170817 had a late onset at $\sim$9 days (Margutti et al. 2017; Troja et al. 2017) and a steady brightening up to $\sim$100 days (Hallinan et al. 2017; Lyman et al. 2018; Mooley et al. 2018c; Ruan et al. 2018). The afterglows from classical short GRBs are typically detected shortly after prompt emission and display a general decline (sometimes accompanied with short-lived plateaus and flares; Fong et al. 2015).

Two leading models were proposed to explain these exceptional behaviors of GW170817: a relativistic structured jet viewed off-axis (Kathirgamaraju et al. 2017; Lamb & Kobayashi 2017; Alexander et al. 2018; Beniamini et al. 2018; D'avanzo et al. 2018; Gill & Granot 2018; Lazzati et al. 2018; Lyman et al. 2018; Margutti et al. 2018; Resmi et al. 2018; Troja et al. 2018; Xie et al. 2018), and a mildly relativistic quasi-spherical outflow (Bromberg et al. 2017; Gottlieb et al. 2017; Kasliwal et al. 2017; Hotokezaka et al. 2018; Mooley et al. 2018c; Nakar et al. 2018; Xie et al. 2018). A heated debate concerning the post-merger outflow structure was raised because these two models, though significantly different, both succeeded in explaining the observed late onset and early brightening.

Wu & MacFadyen (2018) analyzed the multiband GW170817 afterglow data with the physically motivated analytic two-parameter "boosted fireball" model for the outflow structure after it had expanded many orders of magnitude larger than the scale of the central engine (Duffell & MacFadyen 2013a). This model encompasses a family of outflows with structures varying smoothly from a highly collimated ultra-relativistic jet to an isotropic outflow. By performing Markov Chain Monte Carlo (MCMC) analysis, these two leading outflow structures, along with general outflow structures, can be directly compared and distinguished. The fitting results favored the relativistic structured jet viewed off-axis and the quasi-spherical outflow was ruled out due to significantly larger reduced χ^2.

Several other studies also supported the relativistic structured jet model. Lamb et al. (2018) demonstrated that two models have different behaviors with respect to the decline of the post-peak afterglow. The observed steep decline indicates the relativistic structured jet (Lamb et al. 2018, 2019; van Eerten et al. 2018). Mooley et al. (2018a) and Ghirlanda et al. (2019) reported very long baseline interferometry (VLBI) observations, which indicate a superluminal proper motion of the radio counterpart of GW170817.

Given these extensive studies, it is generally accepted that GW170817 has a relativistic jet-like structure, which leads us to ask: if GW170817 is a typical short GRB viewed off-axis, do GW170817 and short GRBs, in general, share similar outflow structures? Are all cosmological short GRBs neutron star mergers?

In this Letter, we present a comprehensive comparison between GW170817 and the short GRB population. We apply the same tools developed in Wu & MacFadyen (2018) and directly compare the outflow structures of GW170817 with those of a sample population of short GRBs (Fong et al. 2015). In Section 2, we give a brief overview of the boosted fireball model. Section 3 describes the data set of 27 cosmological short GRBs. The results are summarized in Section 4 and discussed in Section 5.

2. Method

The idea of a boosted fireball model is that a fireball of specific internal energy η_0 is launched with a boost Lorentz factor γ_B (for details see Duffell & MacFadyen 2013b; Wu & MacFadyen 2018). Due to relativistic beaming, the outflow has a characteristic Lorentz factor $\Gamma \sim 2\eta_0\gamma_B$ and a characteristic jet opening angle $\theta_0 \sim 1/\gamma_B$. Depending on the two parameters, η_0 and γ_B, a family of outflow structures can be generated, from a highly collimated ultra-relativistic jet to an isotropic fireball. Because of its flexibility, the boosted fireball model can serve as a generic outflow model, which is suitable for investigating a population of cosmological short GRBs.

To study the evolution of boosted fireballs expanding in the interstellar medium (ISM), we perform 2D relativistic hydrodynamic simulations using the moving-mesh code `Jet` (Duffell & MacFadyen 2013a). The radial motion of grid cells and adaptive mesh refinement allow us to capture flow structures with high resolution and evolve flows with large Lorentz factors. We employ a standard synchrotron radiation model (Sari et al. 1998) to compute synchrotron radiation from electrons accelerated at the forward shock. To calculate the observed light curve, radiation is collected at the position of observer. For simplicity, we do not consider inverse Compton and synchrotron self-absorption effects on synchrotron spectrum, which may potentially affect synthetic light curves (Fan & Piran 2006; Beniamini et al. 2015).

The parameter space of the boosted fireball model consists of hydrodynamic parameters (η_0, γ_B, the explosion energy E_0, and the ISM density n_0), radiation parameters (the spectral index p, the electron energy fraction ϵ_e, and the magnetic energy fraction ϵ_B), and observational parameters (the observation angle $\theta_{\rm obs}$). By performing a Markov Chain Monte Carlo (MCMC) analysis in this parameter space, we can explore a family of outflows viewed from different observation angles and automatically find the best-fitting parameters.

To enhance fitting performance, E_0 and n_0 are made dimensionless, $E_{0,50} \equiv E_0/10^{50}\,{\rm erg}$ and $n_{0,0} \equiv n_0/1\,{\rm proton\,cm^{-3}}$, and are transformed into a logarithmic scale. The boundaries of the parameter space are $\log_{10} E_{0,50} = [-6,\ 3]$, $\log_{10} n_{0,0} = [-6,\ -1]$, $\eta_0 = [2,\ 10]$, $\gamma_B = [1,\ 12]$, $\theta_{\rm obs} = [0,\ 1]$, $\log_{10}\epsilon_e = [-6,\ 0]$, $\log_{10}\epsilon_B = [-6,\ 0]$, and $p = [2,\ 3]$. Because most short GRBs occur in a low-density environment (Fong et al. 2015), we assume that the ISM has a constant density and set the boundaries of density to be $\log_{10} n_{0,0} = [-6,\ -1]$. The upper boundaries of η_0 and γ_B are limited by the expense of the hydrodynamics simulations. Higher Lorentz factors are computationally expensive for parameter space study. Considering the fact that quasi-spherical outflows usually have wide opening angles corresponding to $\gamma_B \sim 1$–2, our parameter space is large enough to distinguish jet-like and quasi-spherical structures.

By making use of the scaling relations in the hydrodynamic and radiation equations (Van Eerten & MacFadyen 2012; Ryan et al. 2015), we are able to generate synthetic light curves in milliseconds, which allows us to perform MCMC fitting in a reasonable amount of time. However, scaling relations also result in degeneracies between E_0, n_0, ϵ_e, and ϵ_B. In practice, we observe broad posterior distributions for these parameters. Even though degenerate parameters exist in our analysis, other parameters (η_0, γ_B, $\theta_{\rm obs}$, and p) are robustly constrained. The uncertainties of degenerate parameters can be incorporated into the marginalized distributions of non-degenerate parameters. In Wu & MacFadyen (2018), we demonstrated that the medians of marginalized distributions under two scenarios, free and fixed density, were consistent.

Samples are generated by the parallel-tempered affine-invariant ensemble sampler implemented in the `emcee` package (Goodman & Weare et al. 2010; Foreman-Mackey et al. 2013). We set 10 temperature levels and 100 walkers per level for the sampler. The walkers are initialized in a small ball near the maximum of the posterior, calculated through trial runs. We drop the first 5000 steps as burn-in and perform analysis on the following 5000 steps.

3. Data

We consider a catalog of afterglow observations, consisting of all short GRBs from 2004 November to 2015 March with prompt follow-up observations (Fong et al. 2015). The details about the observational data can be found in the Appendix in Fong et al. (2015). Redshifts of these bursts span from $z = 0.12$ to $z = 2.6$. The observational data of GW170817 is taken from Alexander et al. (2018), Margutti et al. (2018), and van Eerten et al. (2018).

Afterglow light curves of short GRBs are sometimes subject to early-time effects, such as steepenings (GRBs 051221A and 111020A), plateaus (GRB 051221A), and flares (GRBs 050724A and 111121A). As the boosted fireball model assumes that the outflow has already expanded far from the central engine, it is not designed to explain these early-time features, which could contaminate the afterglow emission and significantly affect the fit. After these early-time effects are removed, the fitting results are robust. Thus, we trim the early light curves to ensure that the model is applied to the appropriate regime.

Due to the small number of well-observed short GRB afterglows, we would like to include as many short GRBs as possible. Even though fits are performed in an 8D parameter space, we restrict our analysis to all known 27 short GRBs with at least six data points. For 13 short GRBs that do not have a determined spectroscopic redshift, we assume $z = 0.46$, set by the median of the short GRBs with known redshifts (Fong et al. 2017). Of the 27 short GRBs, there are 26 X-ray detections, 23 optical/near-infrared detections, and four radio detections. Four bursts have detections in all three bands. Eighteen bursts have both X-ray and optical/near-infrared detections. Five bursts are detected in only one band.

4. Results

4.1. Goodness of Fit

We perform MCMC analysis on the afterglow light curves of GW170817 and 27 short GRBs. The quality of the fits varied from burst to burst. For light curves with enough data points,

Table 1
Parameter Constraints for GW170817 and the 14 Cosmological Short GRBs

	η_0	γ_B	$\theta_{\rm obs}$	p	θ_0	Γ	$\log_{10} E_{0,50}$	$\log_{10} n_{0,0}$	$\log_{10} \epsilon_e$	$\log_{10} \epsilon_B$
GW170817[a]	$7.9^{+1.3}_{-1.4}$	$9.4^{+1.7}_{-2.1}$	$0.529^{+0.129}_{-0.072}$	$2.15^{+0.01}_{-0.01}$	$0.11^{+0.02}_{-0.03}$	149^{+57}_{-54}	$-0.2^{+0.8}_{-0.8}$	$-2.0^{+0.7}_{-1.0}$	$-1.0^{+0.6}_{-0.9}$	$-3.6^{+1.3}_{-1.4}$
050709	$9.4^{+0.4}_{-0.8}$	$4.5^{+1.0}_{-0.5}$	$0.126^{+0.008}_{-0.012}$	$2.87^{+0.01}_{-0.01}$	$0.22^{+0.04}_{-0.03}$	85^{+23}_{-15}	$-0.1^{+0.4}_{-0.6}$	$-1.6^{+0.4}_{-0.6}$	$-0.3^{+0.2}_{-0.3}$	$-3.4^{+0.9}_{-0.9}$
050724A	$9.0^{+0.8}_{-2.4}$	$11.2^{+0.6}_{-1.3}$	$0.025^{+0.019}_{-0.014}$	$2.24^{+0.14}_{-0.18}$	$0.09^{+0.00}_{-0.01}$	200^{+29}_{-70}	$-1.1^{+0.1}_{-0.1}$	$-1.2^{+0.2}_{-0.3}$	$-0.4^{+0.1}_{-0.1}$	$-2.2^{+0.3}_{-0.3}$
060313	$9.6^{+0.3}_{-0.9}$	$9.5^{+0.5}_{-0.7}$	$0.007^{+0.006}_{-0.004}$	$2.09^{+0.04}_{-0.03}$	$0.10^{+0.01}_{-0.01}$	183^{+16}_{-29}	$-1.4^{+0.1}_{-0.1}$	$-1.1^{+0.1}_{-0.1}$	$-0.1^{+0.1}_{-0.1}$	$-1.7^{+0.1}_{-0.1}$
061006	$7.8^{+1.6}_{-2.1}$	$5.6^{+2.8}_{-2.7}$	$0.158^{+0.093}_{-0.068}$	$2.25^{+0.25}_{-0.16}$	$0.18^{+0.06}_{-0.16}$	88^{+70}_{-54}	$-0.6^{+0.7}_{-0.6}$	$-1.5^{+0.4}_{-0.6}$	$-0.6^{+0.4}_{-0.8}$	$-0.9^{+0.6}_{-0.6}$
061201	$6.3^{+2.6}_{-3.3}$	$7.1^{+4.1}_{-4.1}$	$0.149^{+0.232}_{-0.133}$	$2.55^{+0.27}_{-0.34}$	$0.14^{+0.05}_{-0.19}$	90^{+111}_{-71}	$0.5^{+1.6}_{-2.1}$	$-1.9^{+0.7}_{-1.4}$	$-0.8^{+0.6}_{-1.1}$	$-1.2^{+0.8}_{-1.9}$
070724A	$7.3^{+1.9}_{-2.3}$	$6.5^{+3.1}_{-2.7}$	$0.100^{+0.070}_{-0.047}$	$2.39^{+0.30}_{-0.24}$	$0.15^{+0.05}_{-0.11}$	95^{+81}_{-57}	$-0.8^{+0.9}_{-0.6}$	$-1.4^{+0.3}_{-0.4}$	$-0.6^{+0.4}_{-0.8}$	$-0.5^{+0.4}_{-0.6}$
070809	$7.9^{+1.4}_{-2.1}$	$7.7^{+1.7}_{-1.8}$	$0.045^{+0.035}_{-0.026}$	$2.05^{+0.05}_{-0.03}$	$0.13^{+0.02}_{-0.04}$	122^{+53}_{-53}	$-1.4^{+0.5}_{-0.4}$	$-1.2^{+0.2}_{-0.4}$	$-0.2^{+0.2}_{-0.4}$	$-2.1^{+0.4}_{-0.6}$
080426	$9.9^{+0.1}_{-0.2}$	$11.1^{+0.6}_{-0.7}$	$0.004^{+0.003}_{-0.002}$	$2.24^{+0.11}_{-0.08}$	$0.09^{+0.00}_{-0.01}$	219^{+15}_{-18}	$-2.0^{+0.1}_{-0.1}$	$-1.0^{+0.0}_{-0.1}$	$-0.0^{+0.0}_{-0.1}$	$-0.4^{+0.3}_{-0.4}$
090510	$8.9^{+0.9}_{-2.2}$	$9.2^{+2.0}_{-1.5}$	$0.016^{+0.019}_{-0.010}$	$2.15^{+0.10}_{-0.07}$	$0.11^{+0.02}_{-0.02}$	164^{+55}_{-60}	$-2.0^{+0.3}_{-0.2}$	$-1.1^{+0.1}_{-0.2}$	$-0.1^{+0.1}_{-0.2}$	$-1.3^{+0.3}_{-0.2}$
091109B	$7.7^{+1.6}_{-2.4}$	$9.1^{+2.0}_{-2.3}$	$0.049^{+0.028}_{-0.021}$	$2.13^{+0.10}_{-0.08}$	$0.11^{+0.02}_{-0.04}$	140^{+65}_{-69}	$1.6^{+0.9}_{-1.1}$	$-3.0^{+0.9}_{-1.1}$	$-1.4^{+0.9}_{-1.1}$	$-2.9^{+1.6}_{-1.9}$
110112A	$7.1^{+2.1}_{-2.0}$	$8.6^{+2.1}_{-1.9}$	$0.044^{+0.029}_{-0.024}$	$2.13^{+0.13}_{-0.09}$	$0.12^{+0.02}_{-0.03}$	122^{+74}_{-54}	$-1.7^{+0.5}_{-0.3}$	$-1.3^{+0.2}_{-0.5}$	$-0.3^{+0.2}_{-0.5}$	$-1.0^{+0.4}_{-0.4}$
111020A	$9.0^{+0.7}_{-1.6}$	$9.7^{+1.4}_{-1.4}$	$0.027^{+0.026}_{-0.016}$	$2.04^{+0.15}_{-0.03}$	$0.10^{+0.01}_{-0.02}$	175^{+40}_{-51}	$0.4^{+0.7}_{-0.8}$	$-1.6^{+0.4}_{-0.7}$	$-1.4^{+0.8}_{-0.8}$	$-0.7^{+0.5}_{-0.7}$
111121A	$6.9^{+2.2}_{-2.8}$	$10.0^{+1.3}_{-2.0}$	$0.028^{+0.018}_{-0.013}$	$2.27^{+0.32}_{-0.19}$	$0.10^{+0.01}_{-0.02}$	138^{+67}_{-72}	$2.2^{+0.6}_{-0.9}$	$-3.2^{+0.6}_{-1.0}$	$-0.7^{+0.5}_{-0.8}$	$-2.9^{+1.3}_{-1.4}$
121226A	$3.2^{+2.0}_{-0.8}$	$10.8^{+0.9}_{-1.4}$	$0.026^{+0.011}_{-0.011}$	$2.27^{+0.33}_{-0.19}$	$0.09^{+0.01}_{-0.01}$	68^{+52}_{-24}	$2.0^{+0.7}_{-1.4}$	$-2.2^{+0.7}_{-0.9}$	$-0.6^{+0.4}_{-0.8}$	$-3.2^{+1.8}_{-1.5}$
Mean $\pm$ Std[b]	7.8 ± 1.7	8.6 ± 2.1	0.057 ± 0.052	2.26 ± 0.22	0.12 ± 0.04	135 ± 47	-0.3 ± 0.4	-1.7 ± 0.7	-0.5 ± 0.4	-1.7 ± 1.0

Notes.
[a] We have corrected the medians in Wu & MacFadyen (2018), which misreported the peaks of posterior distributions as the medians.
[b] Means and standard deviations are calculated from the 14 cosmological short GRBs.

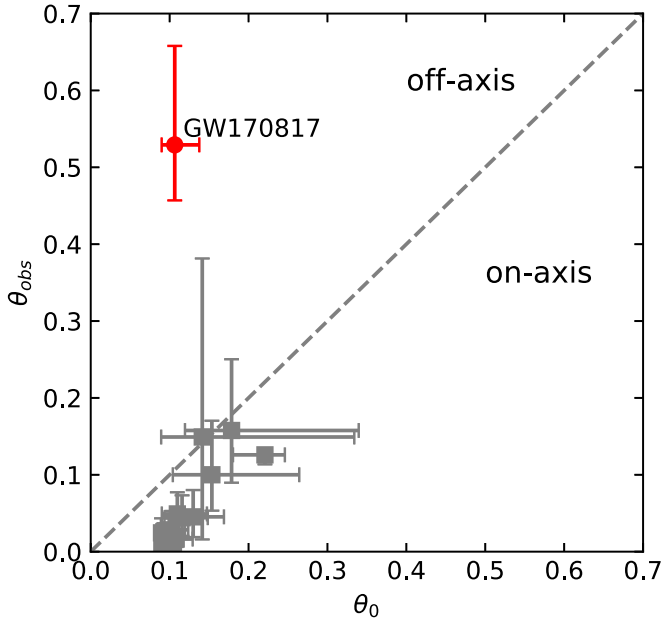

Figure 1. Fit results of jet opening angle θ_0 and observation angle $\theta_{\rm obs}$ for GW170817 (red circle) and 14 short GRBs (blue squares) in the plane (θ_0, $\theta_{\rm obs}$). Jet opening angles are estimated as $\theta_0 \sim 1/\gamma_B$. Markers with error bars indicate median values and symmetric 68% quantiles. The gray dashed line indicates $\theta_{\rm obs} = \theta_0$.

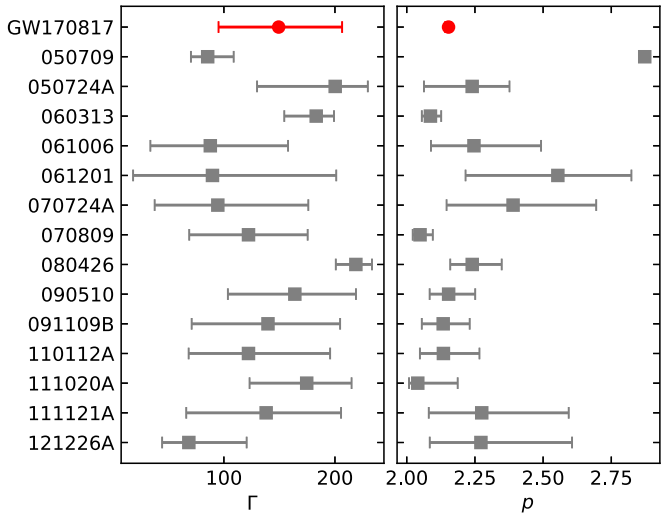

Figure 2. Fit results of the characteristic Lorentz factor Γ (left) and the spectral index p (right) for GW170817 (red circle) and 14 short GRBs (blue squares). Markers with error bars indicate median values and symmetric 68% quantiles.

we can use χ^2/degree of freedom (DOF) to determine the goodness of fit. To be counted as a good fit, we require $\chi^2/{\rm DOF} \leqslant 3$ for bursts with enough data points. Because we allow the number of data points to be less than the number of dimensions of the parameter space in order to incorporate more bursts, the DOFs can be zero or even negative, which makes $\chi^2/{\rm DOF}$ meaningless. Thus, we use χ^2 to determine the goodness of fit and require $\chi^2 \leqslant 10$ for a good fit. However, there are cases with low χ^2 or $\chi^2/{\rm DOF}$, but the fitting light curves are choppy and subject to overfitting, which we consider bad fits.

We find that GW170817 and 14 bursts have reasonably good fits. For 13 bursts, we are unable to find good fits. There are several factors that could lead to a low-quality fit: lack of

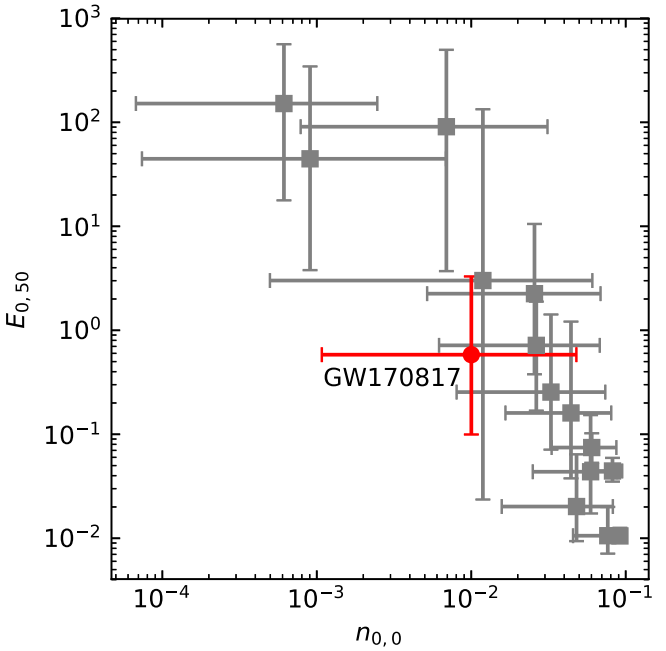

Figure 3. Fit results of explosion energy $E_{0,50}$ and ISM density $n_{0,0}$ for 14 short GRBs (blue squares) and GW170817 (red circle). Markers with error bars indicate median values and symmetric 68% quantiles.

enough data points, too much noise in the data, the quality of synthetic light curves, and violations of model assumptions such as homogeneous ISM. To serve as an example of a good fit, the contour plots and best-fitting light curves for GW170817 can be found in Wu & MacFadyen (2018).

4.2. Constraints on Fitting Parameters

In Table 1, we show the constraints of fitting parameters (η_0, γ_B, $\theta_{\rm obs}$, p, $E_{0,50}$, $n_{0,0}$, ϵ_e, ϵ_B) and corresponding characteristic parameters (θ_0, Γ) for GW170817 and 14 good fit bursts. In Figure 1, we show the distribution of GW170817 (red circle) and 14 short GRBs (blue squares) in the (θ_0, $\theta_{\rm obs}$) plane. GW170817 is found to have a jet opening angle $\theta_0 = 0.11^{+0.02}_{-0.01}$ rad $= 6.3^{+1.1}_{-0.6}{}^\circ$, which is consistent with those from other studies (Mooley et al. 2018a; Pooley et al. 2018; van Eerten et al. 2018). Remarkably, all short GRBs are also found to have similar jet-like outflows. The mean and standard deviation of jet opening angles is 0.12 ± 0.04 rad $= 6.^\circ9 \pm 2.^\circ3$, which is consistent with that of GW170817. The range of jet opening angle for short GRBs is also consistent with Beniamini et al. (2018)s estimation $\theta_0 \approx 0.1$ from comparing rates between cosmological short GRBs and neutron star mergers For bursts with distinct jet breaks, jet opening angles can be estimated from the observed jet breaks. Fong et al. (2015) estimated the jet opening angle ($\theta_0 = 3^\circ$–8°) for GRB 111020A from its jet break, which is consistent with our value $\theta_0 = 4.^\circ7$–$6.^\circ5$. θ_0 may be lower because it is limited by the upper boundary of $\gamma_{B,\rm max} = 12$, which corresponds to $\theta_{0,\ \rm min} = 0.08$ rad $= 4.^\circ6$. GW170817 and short GRBs share the same outflow structures with $\gamma_B \gtrsim 9$ corresponding to structured jets, and are outside the range $\gamma_B = 1$–2 corresponding to quasi-spherical outflows.

For GW170817, the observation angle $\theta_{\rm obs} = 0.53$ rad $= 30^\circ$ is significantly larger than $\theta_0 = 0.11$ rad $= 6.^\circ3$, which indicates that it is viewed significantly off-axis, outside of the jet opening angle. Mooley et al. (2018a) and van Eerten et al. (2018) also found a significant off-axis observation angle

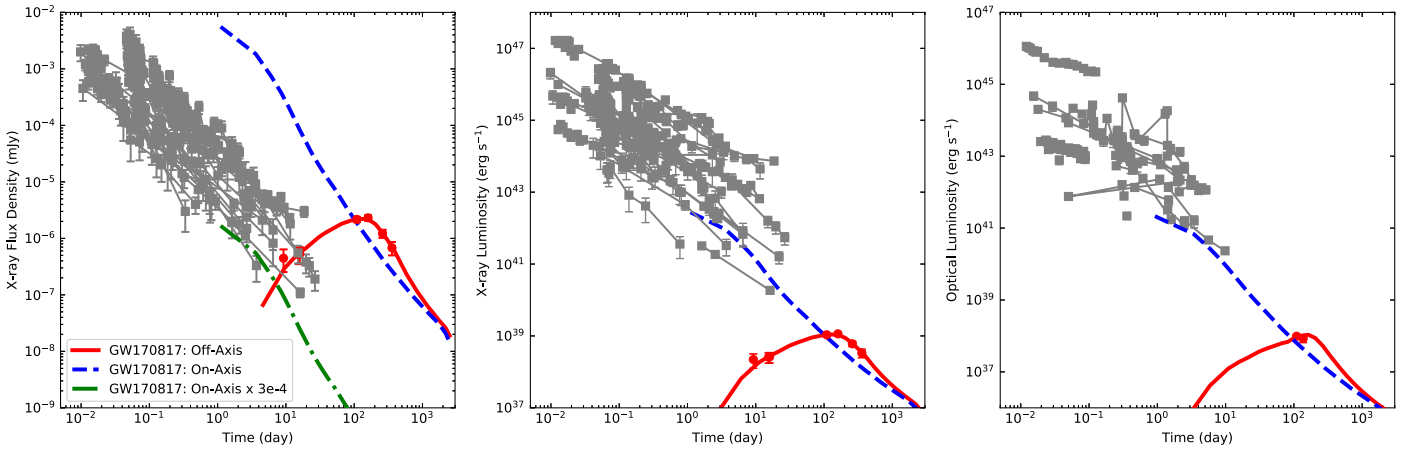

Figure 4. X-ray flux density (left panel), X-ray luminosity (middle panel), and optical luminosity (right panel) for GW170817 (red circles with error bars) and 27 cosmological short GRBs (gray squares with error bars). Red solid line: the best-fitting light curve ($\theta_{\rm obs} = 0.53$ rad $= 30°$). Blue dashed line: the on-axis light curve obtained by setting $\theta_{\rm obs} = 0$. Green dashed–dotted line: the on-axis light curve adjusted by an inverse square distance factor of 3×10^{-4}.

for GW170817. For short GRBs, the mean and standard deviation of observation angles is 0.06 ± 0.05 rad ($3\overset{\circ}{.}4 \pm 2\overset{\circ}{.}9$). In Figure 1, short GRBs (blue squares) are located below the dashed gray line ($\theta_{\rm obs} = \theta_0$), which indicates that the line of sight is located inside the cone of the outflow. We note that GW170817 is the nearest event ($z = 0.00973$). After the detection of the gravitational-wave signal, it attracted significant attention from the community and was monitored intensively. On the other hand, the 14 short GRBs are cosmological ($z = 0.12$–2.6). The significant difference of observation angles between GW170817 and cosmological short GRBs can be explained by observation bias. Most cosmological short GRBs are detected on-axis; otherwise, they would be too weak to be conclusively detected. The observations of γ-rays and afterglows can be used to constrain the angular structures of energy and Lorentz factor (Beniamini & Nakar 2018), which are consistent with our results.

In Figure 2, we show the fitting results of the characteristic Lorentz factor ($\Gamma \sim 2\eta_0\gamma_B$) for GW170817 and 14 short GRBs. GW170817 has $\Gamma \approx 150$, which fits well within the range of short GRBs ($\Gamma = 135 \pm 47$). For GW170817, the Lorentz factor long the line of sight to the observer is 5.3, which fits the expectation that the early emission is effectively dominated by radiation from mildly relativistic material.

In Figure 2, we show the fitting results of the spectral index p. GW170817 has a tight constraint $p = 2.15^{+0.01}_{-0.01}$, as it has good observational data from all three bands. The mean and standard deviation of short GRBs is $p = 2.26 \pm 0.22$. The spectral index of GW170817 is consistent with those of short GRBs.

Figures 3 shows the distributions of GW170817 and 14 short GRBs in the ($n_{0,0}$, $E_{0,50}$) plane. GW170817 has $n_0 \approx 10^{-2}$ proton cm^{-3} and $E_0 \approx 6 \times 10^{49}$ erg. Considering the jet opening angle $\theta_0 \approx 0.11$ rad, the corresponding isotropic equivalent energy is $E_{\rm iso} \approx 8 \times 10^{52}$ erg. These values are located within the typical ranges of short GRBs. Because $n_{0,0}$ and $E_{0,50}$ are degenerate parameters, most of the bursts display large error bars. Due to the scaling relations, our model is better at constraining outflow structures rather than estimating accurate values of degenerate parameters. Even though these degenerate parameters are not well constrained, we note that their uncertainties can be marginalized out, and thus will not affect the constraints on non-degenerate parameters. In Wu & MacFadyen (2018), we broke the degeneracies by fixing density as $n_{0,0} = 10^{-3}$, and the outflow structure of GW170817 remains consistent. The values of ϵ_e for the short GRBs is found to be around 0.3, which is consistent with other studies (Cenko et al. 2010; Beniamini & van der Horst 2017).

4.3. On-axis Light Curves

We have found that GW170817 and short GRBs share similar outflow structures and other physical parameters, except for the observation angle. Viewed off-axis, GW170817 displayed exceptional behaviors, such as late onset and early brightening. Short GRBs are viewed on-axis and show a general decline shortly after prompt emission. This leads to an interesting question: what would be observed from GW170817 if the observer were located on-axis?

In Figure 4, we show the X-ray afterglow observations for GW170817 (red circles with error bars) and 27 cosmological short GRBs (gray squares with error bars). The best-fitting light curve for GW170817 (red solid line) fits the observational data very well. It captures the late onset at around ∼9 days, the steady brightening up to ∼100 days, and the turnover at ∼150 days.

Given the set of best-fitting parameters for GW170817, we can generate the on-axis light curve by setting $\theta_{\rm obs} = 0$ and leaving all other parameters unchanged. The resulting on-axis light curve is shown in blue dashed line in Figure 4. It shows a monotonic decline, just like other short GRBs. At late times, the on-axis light curve coincides with the off-axis light curve. This is due to the whole region of the decelerated outflow becoming observable for both on-axis and off-axis observers.

GW170817 is a local event ($d_L = 39.5$ Mpc), therefore its flux density is significantly higher than others. The median redshift for short GRBs is $z = 0.46$ (Fong et al. 2017). Using a benchmark ΛCDM cosmology with $H_0 = 71$ km s^{-1} Mpc^{-1} and $\Omega_m = 0.27$, the corresponding luminosity distance can be calculated as $d_L \sim 2500$ Mpc. The inverse square factor can be roughly estimated as 3×10^{-4}. The on-axis light curve adjusted for the inverse square factor is shown as the green dashed–dotted line. Though located a little lower, it is consistent with the observations from short GRBs. To better compare the intrinsic properties, we also show the X-ray and

optical luminosity as a function of time in Figure 4. The on-axis light curve from GW170817 is located in the middle of light curves from the short GRB population. This reveals that GW170817 is intrinsically similar to short GRBs. The differences between GW170817 and short GRBs are mainly due to extrinsic properties, such as observation angle and redshift.

Recently, Salafia et al. (2019) computed afterglow light curves from GW170817 with a power-law-structured jet model and compared it with a population of short GRBs from Fong et al. (2015). They found that the on-axis light curve from GW170817 falls in the middle of the observed population of short GRB afterglows, which is consistent with our results.

5. Discussion

We systematically compare the properties of GW170817 and a population of short GRBs by performing MCMC analysis in the 8D parameter space of hydrodynamic, radiation, and observational parameters,

We demonstrate that GW170817 and short GRBs share the same outflow structure: a relativistic structured jet. The only difference in our analysis between GW170817 and the cosmological short GRBs is that GW1701817 is viewed off-axis and the cosmological short GRBs are viewed on-axis. The difference in observation angle can explain the exceptional behavior of the GW170817 afterglow light curve, such as the late onset and early brightening. Other properties of the GW170817 afterglow, including jet opening angle, Lorentz factor, and spectral index, are all consistent with those of cosmological short GRBs.

We calculate the light curve for the GW170817 afterglow that on-axis viewers would have observed. It shows a temporal decline that is consistent with cosmological short GRBs. The similarity between GW170817 and short GRBs indicates that cosmological short GRBs are also neutron star mergers.

We are grateful to Michael Blanton, Wen-fai Fong, and Roman Scoccimarro for helpful discussions and comments. This research was supported in part by the NSF through grant AST-1715356.

ORCID iDs

Yiyang Wu https://orcid.org/0000-0002-5347-9225
Andrew MacFadyen https://orcid.org/0000-0002-0106-9013

References

Abbott, B. P., Abbott, R., Abbott, T., et al. 2017, PhRvL, 119, 161101
Alexander, K., Berger, E., Fong, W., et al. 2017, ApJL, 848, L21
Alexander, K. D., Margutti, R., Blanchard, P. K., et al. 2018, ApJL, 863, L18
Beniamini, P., & Nakar, E. 2018, MNRAS, 482, 5430
Beniamini, P., Nava, L., Duran, R. B., & Piran, T. 2015, MNRAS, 454, 1073
Beniamini, P., Petropoulou, M., Barniol Duran, R., & Giannios, D. 2018, MNRAS, 483, 840
Beniamini, P., & van der Horst, A. J. 2017, MNRAS, 472, 3161
Bromberg, O., Tchekhovskoy, A., Gottlieb, O., Nakar, E., & Piran, T. 2017, MNRAS, 475, 2971
Cenko, S., Frail, D., Harrison, F., et al. 2010, ApJ, 711, 641
D'avanzo, P., Campana, S., Salafia, O. S., et al. 2018, A&A, 613, L1
Dobie, D., Kaplan, D. L., Murphy, T., et al. 2018, ApJL, 858, L15
Duffell, P. C., & MacFadyen, A. I. 2013a, ApJ, 775, 87
Duffell, P. C., & MacFadyen, A. I. 2013b, ApJL, 776, L9
Fan, Y., & Piran, T. 2006, MNRAS, 369, 197
Fong, W.-f., Berger, E., Blanchard, P., et al. 2017, ApJL, 848, L23
Fong, W.-f., Berger, E., Margutti, R., & Zauderer, B. A. 2015, ApJ, 815, 102
Foreman-Mackey, D., Hogg, D. W., Lang, D., & Goodman, J. 2013, PASP, 125, 306
Ghirlanda, G., Salafia, O., Paragi, Z., et al. 2019, Sci, 363, 968
Gill, R., & Granot, J. 2018, MNRAS, 478, 4128
Goldstein, A., Veres, P., Burns, E., et al. 2017, ApJL, 848, L14
Goodman, J., Weare, J., et al. 2010, Communications in Applied Mathematics and Computational Science, 5, 65
Gottlieb, O., Nakar, E., & Piran, T. 2017, MNRAS, 473, 576
Haggard, D., Nynka, M., Ruan, J. J., et al. 2017, ApJL, 848, L25
Hallinan, G., Corsi, A., Mooley, K., et al. 2017, Sci, 358, 1579
Hotokezaka, K., Kiuchi, K., Shibata, M., Nakar, E., & Piran, T. 2018, ApJ, 867, 95
Kasliwal, M., Nakar, E., Singer, L., et al. 2017, Sci, 358, 1559
Kathirgamaraju, A., Barniol Duran, R., & Giannios, D. 2017, MNRAS, 473, L121
Lamb, G., Lyman, J., Levan, A., et al. 2019, ApJL, 870, L15
Lamb, G. P., & Kobayashi, S. 2017, MNRAS, 472, 4953
Lamb, G. P., Mandel, I., & Resmi, L. 2018, MNRAS, 481, 2581
Lazzati, D., Perna, R., Morsony, B. J., et al. 2018, PhRvL, 120, 241103
Lyman, J. D., Lamb, G. P., Levan, A. J., et al. 2018, NatAs, 2, 751
Margutti, R., Alexander, K., Xie, X., et al. 2018, ApJL, 856, L18
Margutti, R., Berger, E., Fong, W., et al. 2017, ApJL, 848, L20
Mooley, K., Deller, A., Gottlieb, O., et al. 2018a, Natur, 561, 355
Mooley, K., Frail, D., Dobie, D., et al. 2018b, ApJL, 868, L11
Mooley, K., Nakar, E., Hotokezaka, K., et al. 2018c, Natur, 554, 207
Nakar, E., Gottlieb, O., Piran, T., Kasliwal, M. M., & Hallinan, G. 2018, ApJ, 867, 18
Nynka, M., Ruan, J. J., Haggard, D., & Evans, P. A. 2018, ApJL, 862, L19
Piro, L., Troja, E., Zhang, B., et al. 2018, MNRAS, 483, 1912
Pooley, D., Kumar, P., Wheeler, J. C., & Grossan, B. 2018, ApJL, 859, L23
Resmi, L., Schulze, S., Ishwara-Chandra, C., et al. 2018, ApJ, 867, 57
Ruan, J. J., Nynka, M., Haggard, D., Kalogera, V., & Evans, P. 2018, ApJL, 853, L4
Ryan, G., Van Eerten, H., MacFadyen, A., & Zhang, B.-B. 2015, ApJ, 799, 3
Salafia, O. S., Ghirlanda, G., Ascenzi, S., & Ghisellini, G. 2019, arXiv:1905.01190
Sari, R., Piran, T., & Narayan, R. 1998, ApJL, 497, L17
Savchenko, V., Ferrigno, C., Kuulkers, E., et al. 2017, ApJL, 848, L15
Troja, E., Piro, L., Ryan, G., et al. 2018, MNRAS, 478, L18
Troja, E., Piro, L., van Eerten, H., et al. 2017, Natur, 551, 71
van Eerten, E. T. H., Ryan, G., Ricci, R., et al. 2018, arXiv:1808.06617
Van Eerten, H. J., & MacFadyen, A. I. 2012, ApJL, 747, L30
Wu, Y., & MacFadyen, A. 2018, ApJ, 869, 55
Xie, X., Zrake, J., & MacFadyen, A. 2018, ApJ, 863, 58
Zrake, J., Xie, X., & MacFadyen, A. 2018, ApJL, 865, L2